Supporting Information

Hydrogen bond interactions on the dual-core copper catalyst promote the activation of low-concentration CO_2 and the generation of ethylene

Guodong Sun, [a, b*] Yingfei Ma,[a, b] Yanan Cao,[c] Kaiyang Zhao,[a] Kewen Ao, [a] Xinqi Wang, [a] Mingtian Hao[d], Mengchen Sun[e], and Wei Zhang[a*]

Supplementary Index

Experimental section

Table S6. The charge transfer resistance of $[Cu_2(OH)_2L_2]$-X catalysts.
Table S7 Comparison of catalytic performance of some dual-core Cu catalysts
Table S8. Calculated Electronic Energies and Gibbs Free Energies in Hartree.

Reagents and materials.

Copper chloride ($CuCl_2·2H_2O$, 99.0 %) was purchased from Beijing Chemical Plant Co., LTD. 2,2'-Bipyridine ($C_{10}H_8N_2$, 99.0 %, denoted as Bipy), deuterium oxide (D_2O, 99.9%), potassium hydroxide (KOH, 95.0 %) were purchased from Shanghai Maclin Biochemical Co., LTD. 1,10-Phenanthroline ($C_{12}H_8N_2·H_2O$, 99.0 %, denoted as Phen) was purchased from Beijing Ruida Henghui Technology Development Co., LTD. Ethanol (C_2H_5OH, 99.8 %), ammonia ($NH_3·H_2O$, 25.0 %~28.0 %), and terephthalic acid ($C_8H_6O_4$, 98.5 %) were purchased from Sinophosphate Holding Chemical Reagent Co., LTD. Methanol (CH_3OH, 99.5 %) and Acetone (C_3H_6O, 99.5 %) were purchased from Beijing Tongguang Fine Chemical Company. Carbon paper was purchased from Toray Industries. Nafion 117 membranes are sourced from Dupont™. The 18.2 MΩ cm ultrapure water was obtained from the milli-Q system. Carbon dioxide gas (purity 99.999 %) and argon gas (purity 99.999 %) were purchased from Beijing Millennium Capital Gas Co., LTD. All chemicals were used as is without further purification.

Syntheses of catalysts

The synthesis of the two catalysts was based on the previous methods with some modifications.[1–2]

Synthesis of $[Cu_2(OH)_2(Phen)_2](pta)$: $CuCl_2·2H_2O$ (0.170 g, 1.00 mmol) was dissolved in 5.0 mL of H_2O, and 1.0 mL of Na_2CO_3 solution (1 M) was added drop by drop during agitation. The blue precipitate obtained was washed and centrifugated three times.

The precipitate was then transferred to a solution ($V_{methanol}$: V_{water} =1:1, 50 mL), to which 1,10-Phenanthroline monohydrate (0.198 g, 1.00 mmol) and terephthalic acid (0.166 g, 1.00 mmol) were added in turn. $NH_3 \cdot H_2O$ was added drop by drop to the above mixture solution until pH = 12.8. The clear solution is placed in a 100 mL Teflon-lined autoclave and heated at 100 °C for 72 hours to obtain the product. (Chemical formula: $C_{32}H_{42}Cu_2N_4O_{16.}$ yield: 61.2 %, based on the $CuCl_2 \cdot 2H_2O$).

Synthesis of $[Cu_2(OH)_2(Bipy)_2](Hba)_2$: $CuCl_2 \cdot 2H_2O$ (0.170 g, 1.00 mmol) was dissolved in 5.0 mL of H_2O, and 1.0 mL of Na_2CO_3 solution (1 M) was added drop by drop during agitation. The blue precipitate obtained was washed and centrifugated three times. The precipitates were then transferred to a solution ($V_{acetone}$: V_{water} =1:1, 50 mL), to which 2,2'-Bipyridine (0.156 g, 1.00 mmol) and barbituric acid (0.128 g, 1.00 mmol) were added in turn. $NH_3 \cdot H_2O$ was added drop by drop to the above mixture solution until pH = 12.3. The clear solution is placed in a 100 mL Teflon-lined autoclave and heated at 100 °C for 72 hours to obtain the product. (Chemical formula: $C_{28}H_{44}Cu_2N_8O_{18.}$ yield: 52.6 %, based on the $CuCl_2 \cdot 2H_2O$).

Electrochemical measurements

Preparation of cathode electrodes.

2 mg of electrocatalyst was uniformly ground to power and then dispersed into a mixed solution of H_2O (100 μL), anhydrous ethanol (80 μL), and Nafion (20 μL). The mixture was sonicated for 30 minutes to obtain a mixed ink. 100 μL of the catalyst ink was pipetted onto the center (S =1 cm × 1 cm) of a carbon paper electrode (S = 2 cm × 2 cm) with a loading of 1 mg cm^{-2}. The electrode was then slowly dried at room

temperature for subsequent electrochemical testing experiments. In preparing the working electrode, the Nafion solution was used as the dispersion liquid of the electrocatalyst, which facilitates the uniform adhesion of the catalyst on the surface of carbon paper.

Catalytic Evaluation.

The electrochemical tests for CO_2 reduction reaction (CO_2RR) were performed on the electrochemical workstation (DH7001) in a three-channel flow cell consisting of a gas diffusion electrode (GDE), an anion exchange membrane (Fumasep, FAA-PK-130) and a platinum plate. In the electrochemical test, the GDE uniformly coated with electrocatalyst suspension was used as the working electrode, an Hg/HgO electrode was used as the reference electrode, and a Pt plate was used as the counter electrode. The anion exchange membrane separated the cathode and anode chambers. The electrolyte is 0.1 M KOH (pH = 13.0) with injecting Argon gas for 30 minutes to remove oxygen that may dissolve. The cathode and anode electrolytes were circulated by a peristaltic pump (Chuxi-Pump, YZ15) with a flow rate of 10 mL min^{-1}. The high-purity carbon dioxide (99.9995%) gas was continuously diffused through the flow chamber located behind the gas diffusion layer to the electrolyte at the catalyst. The gas flow controller (Sevenstar, D07-19B) is set to control the gas flow to 30 sccm. All potentials were measured versus a Hg/HgO reference electrode without iR compensation, and the results were reported versus a reversible hydrogen electrode (RHE) based on the Nernst equation:

$$E\ (V\ vs.\ RHE) = E\ (V\ vs. Hg/HgO) + 0.0977 + 0.059 \times pH$$

The linear sweep voltammetry (LSV) curve was used to select the appropriate potential range of the catalyst. The sweeping range was from 0 to −1.2 V (vs. RHE) at a scan rate of 50 mV s^{-1} in 0.1 M KOH solution with CO_2/Ar flowing. To estimate the electrochemical active surface area (ECSA), cyclic voltammetry (CV) curves were tested by measuring double-layer capacitance (C_{dl}) with various scan rates from 20 to 200 mV s^{-1}. Before the CV test, the electrolyte was bubbled with Ar for 30 min. All the potentials were measured versus the Hg/HgO electrode, and the results were reported versus the reversible hydrogen electrode (RHE).

Quantitative analysis of gas and liquid products.

A gas chromatography (GC, SP-2100) system was used to analyze the gaseous products from the cell. Liquid-phase products were determined by nuclear magnetic resonance (^{1}H NMR) spectra recorded on an Ascend 400 spectrometer (500 MHz, Bruker, Germany). The outlet of gas in the electrolytic cell was directly connected with a six-way valve in the gas chromatograph through a sealed rubber tube. After the electrolytic reaction ran for at least 300 seconds, the gas products were analyzed by gas chromatography. The liquid products in cathode chambers were collected during electrolysis and analyzed by NMR of a mixed solution of 500 μL electrolyte, 500 μL DMSO, and 100 μL D_2O. Faraday efficiency (FE) was determined by dividing each product's charge generated by the total amount of charge passed during the entire operation or in a specific period. The FE values of the products were calculated by the following formula: FE = $Z \times n \times F / Q_{total}$

Z = the number of electrons transferred (CO, HCOOH, or H_2 is 2; CH_4 is 8; C_2H_4 or

C_2H_5OH is 12);

n = a given product's number of moles;

F = Faraday's constant (96485 $C \cdot mol^{-1}$);

Q_{total} = all the charge passed throughout the electrolysis process.

The isotope-labeled experiments were performed using $^{13}CO_2$ under almost the same conditions as those of $^{12}CO_2$, and the products were analyzed using gas chromatography-mass spectrometry (7890B and 5977B, Agilent) coupled with a GS CarbonPlot capillary column (Agilent).

Characterization.

The crystals were installed in a single crystal diffractometer (SC-XRD, Bruker APEX-II CCD Quest) equipped with cryogenic equipment. Mo Kα radiation was used for examination and data collection (λ = 0.71073 Å). Crystal data were collected, reflections were indexed and processed, and the files were scaled and corrected for absorption using Bruker APEX2. All non-hydrogen atoms were refined with anisotropic displacement parameters and hydrogen positions were fixed at calculated positions and refined isotropically. Using Olex2,[3] the structure was solved with the SHELXT[4] structure solution program using Intrinsic Phasing and refined with the SHELXL refinement package using Least Squares minimization. The measured values of the crystal powders at ambient temperature were recorded by powder X-ray diffraction (XRD, Rigaku SmartLab, Cu Kα radiation, λ= 1.54 Å). The voltage was 40 kV and the current was 40 mA. X-ray photoelectron spectroscopy (XPS) analysis was performed using Al Kα radiation on AXIS SUPRATM X-ray photoelectron spectrometer. Raman

spectra were obtained using 532 nm laser excitation with a laser power of 5 mW on a Renishaw Raman microscope. NMR spectra were recorded with Shimadzu Avance 400 spectrometer at ambient temperature.

Computational Details.

The CO_2 reduction reaction (CO_2RR) mechanism was investigated via density functional theory (DFT) by the Gaussian 09 package,[5] which was widely used in the theoretical study of molecular electrocatalysts in homogeneous [6–7] and heterogeneous catalysis.[8–9] All geometry optimization was accomplished by the PBE0[10] method combined with a mixed basis set (def2-SVP[11–12] basis for all main group elements, SDD [13] basis for Cu). Grimme's DFT-D3(BJ)[14] dispersion correction was applied to embody hydrogen bonds and the long-range van der Waals interactions. Frequency calculations were accomplished at the same level to determine the nature of each stationary point and obtain the Gibbs free energy corrections at 298.15 K and 1 atm. To obtain more accurate free energies, single-point energy calculations were carried out by TPSSh[15] method together with def-TZVP[16] for main group elements and SDD basis set for Cu, while the solvent effect of water was estimated by the implicit solvent model SMD[17–18]. It was worth noting that PBE0 hybrid was in common use for organometallic calculations and TPSSh-D3(BJ) hybrid performed well in organometallic thermochemistry according to previous studies.[19–22] Gibbs free energies were corrected by Shermo[23] code using Grimme's modified harmonic oscillator approximation[24] to better deal with low frequencies.

In consideration of open-shell broken-symmetry singlet, we optimized the geometries of $[Cu_2(OH)_2(Bipy)_2]^{2+}$ (Figure S2) in both singlet and triplet states, and A-COOH in both doublet and quartet states. The distance (D_{Cu-Cu}) between neighboring bi-Cu atoms in the triplet state (2.931 Å) is closer to the experimental value (2.864 Å) reported in previous work.[1] Meanwhile, their triplet and quartet states possess lower Gibbs free energies in comparison to the corresponding singlet and doublet states. Hence, we displayed the computation results of intermediates in s=1 and s=3/2 states below.

For writing simplicity, $[Cu_2(OH)_2(Bipy)_2]^{2+}$ and $[Cu_2(OH)_2(Phen)_2]^{2+}$ were denoted as A and B in this article. Explicit water molecules may affect the calculation results. Therefore, we calculated the reaction free energy of a key endergonic step ($A\text{-}CO_2 + H^+ + e^- = A\text{-}COOH$) over A in the presence of two water molecules (Figure S22). When two water molecules are absent, this step possesses the reaction-free energy of 12.9 kcal mol^{-1}. Meanwhile, when two water molecules are present, the reaction-free energy is 13.2 kcal mol^{-1}. The above calculation results indicate that explicit water can be assumed to have little effect on the reaction, so it is reasonable to consider only the implicit solvent model.

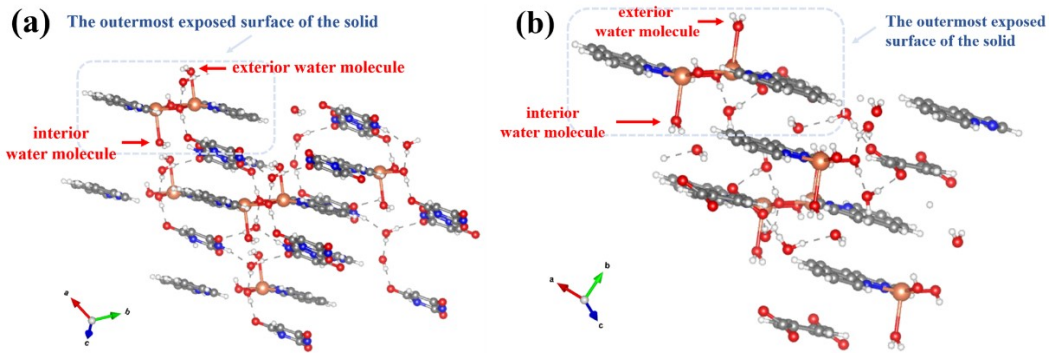

Figure S1. The π···π stacking interaction in the $[Cu_2(OH)_2L_2]$-X. **(a)** $[Cu_2(OH)_2(Bipy)_2](Hba)_2$ **(b)** $[Cu_2(OH)_2(Phen)_2](pta)$. The circled area represents the active site ($[Cu_2(OH)_2L_2]^{2+}$) exposed on the outermost surface of the solid.

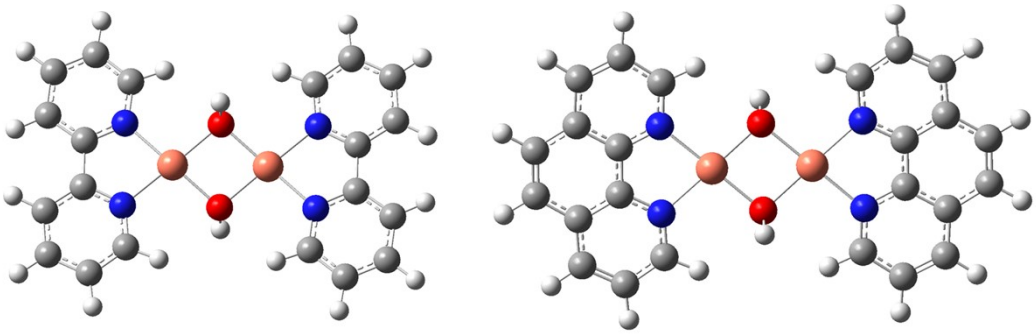

$[Cu_2(OH)_2(Bipy)_2]^{2+}$ $[Cu_2(OH)_2(Phen)_2]^{2+}$

Figure S2. Optimized initial structure models of $[Cu_2(OH)_2(Bipy)_2]^{2+}$ and $[Cu_2(OH)_2(Phen)_2]^{2+}$.

The conceivable pathways for CO_2 reduction to C_2H_4 in this work are listed below:

$$A/B + CO_2 \rightarrow A/B\text{-}CO_2$$
$$A/B\text{-}CO_2 + H^+ + e^- \rightarrow A/B\text{-}COOH$$
$$A/B\text{-}COOH + H^+ + e^- \rightarrow A/B\text{-}CO + H_2O$$
$$A/B\text{-}CO + CO_2 \rightarrow A/B\text{-}(CO + CO_2)$$
$$A/B\text{-}(CO + CO_2) + H^+ + e^- \rightarrow A/B\text{-}(CO + COOH)$$
$$A/B\text{-}(CO + COOH) + H^+ + e^- \rightarrow A/B\text{-}(CO + CO) + H_2O$$
$$A/B\text{-}(CO + CO) + H^+ + e^- \rightarrow A/B\text{-}COCHO$$
$$A/B\text{-}COCHO + H^+ + e^- \rightarrow A/B\text{-}CHOCHO$$
$$A/B\text{-}CHOCHO + H^+ + e^- \rightarrow A/B\text{-}CHOCHOH$$
$$A/B\text{-}CHOCHOH + H^+ + e^- \rightarrow A/B\text{-}CHOCH_2OH$$
$$A/B\text{-}CHOCH_2OH + H^+ + e^- \rightarrow A/B\text{-}CHOCH_2 + H_2O$$
$$A/B\text{-}CHOCH_2 + H^+ + e^- \rightarrow A/B\text{-}CHOHCH_2$$
$$A/B\text{-}CHOHCH_2 + H^+ + e^- \rightarrow A/B\text{-}CH_2OHCH_2$$
$$A/B\text{-}CH_2OHCH_2 + H^+ + e^- \rightarrow A/B\text{-}C_2H_4$$
$$A/B\text{-}C_2H_4 \rightarrow A/B + C_2H_4(g)$$

(A and B represent different catalysts.)

(A and B represent different catalysts.)

Figure. S3. The stepwise reaction equation for catalytic CO_2 reduction.

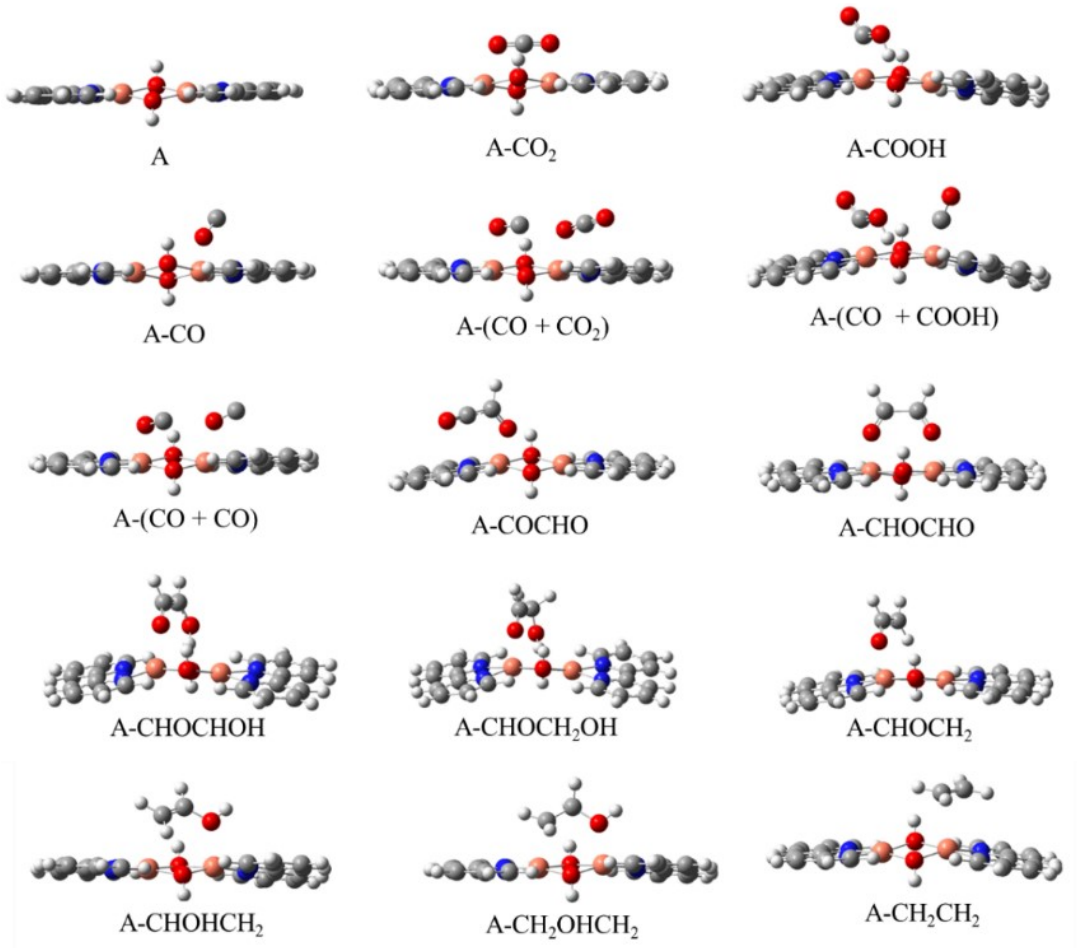

Figure S4. Calculated A structures containing adsorbed species.

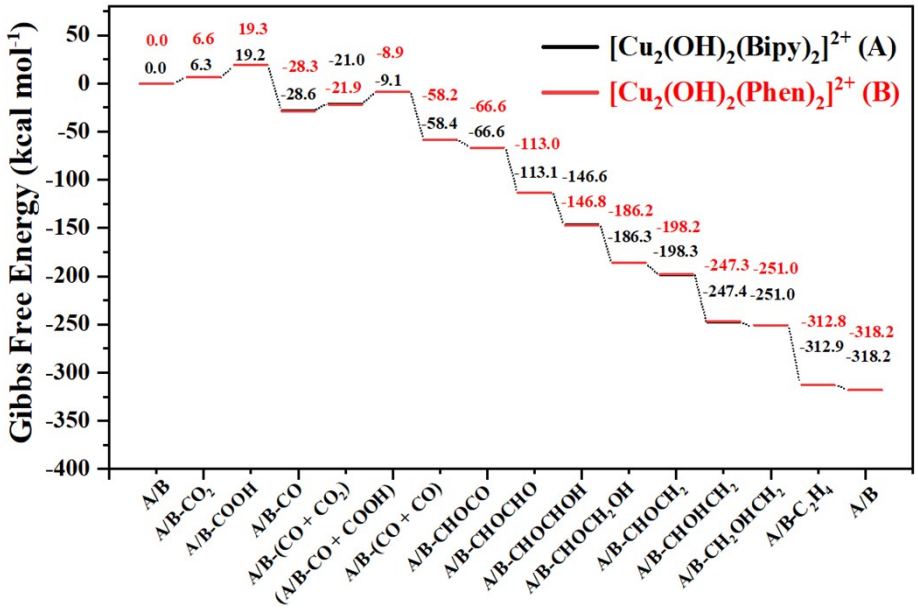

Figure S5. The calculated Gibbs free energy profile of $[Cu_2(OH)_2L_2]^{2+}$ at U = −1.10 V (vs. RHE).

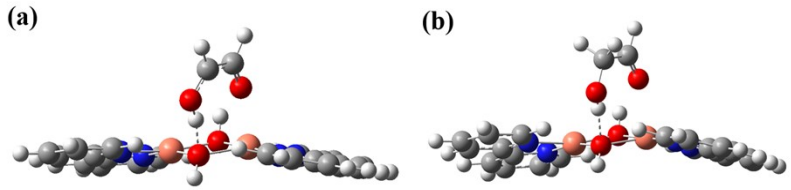

Figure S6. Calculated structures of (a) A-CHOCHOH and (b) A-CHOCH$_2$OH intermediates (with forming hydrogen bonds).

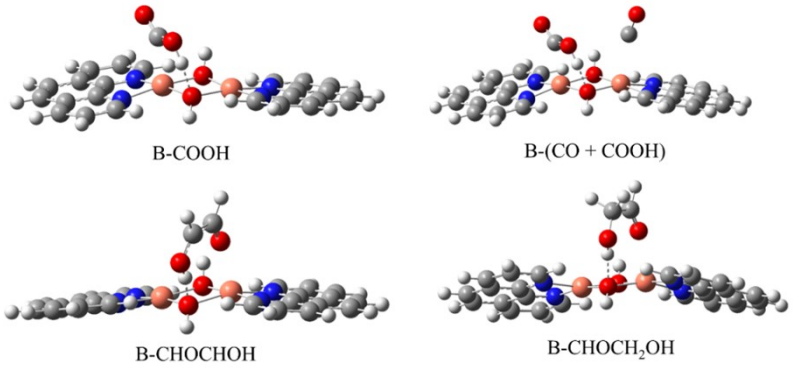

Figure S7. Calculated B structures containing adsorbed species with forming hydrogen bonds.

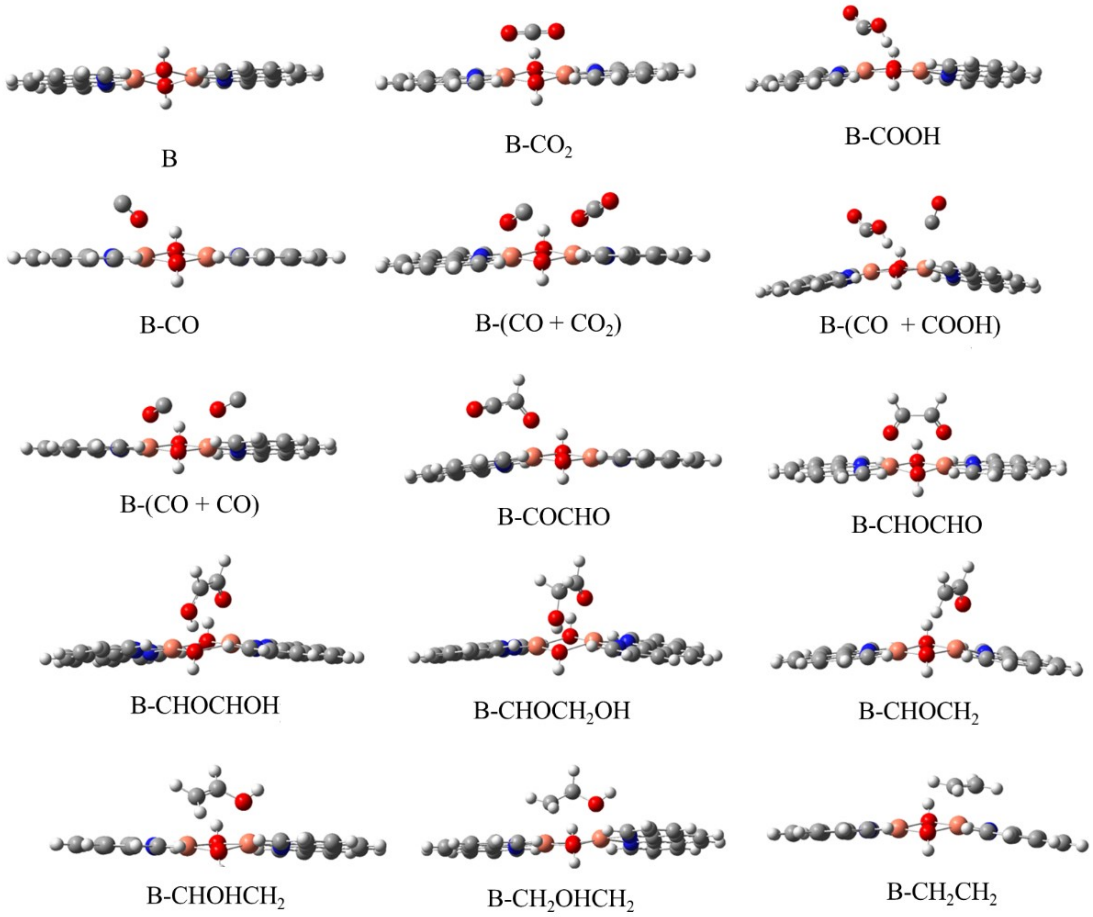

Figure S8. Calculated B structures containing adsorbed species.

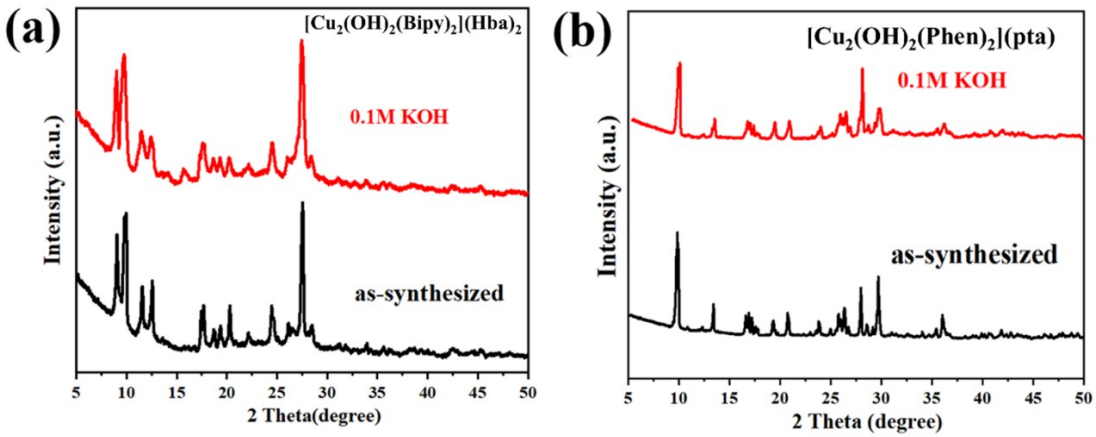

Figure S9. PXRD patterns of $[Cu_2(OH)_2L_2]$-X after soaking in 0.1 M KOH solution for 10 h. **(a)** $[Cu_2(OH)_2(Bipy)_2](Hba)_2$ **(b)** $[Cu_2(OH)_2(Phen)_2](pta)$.

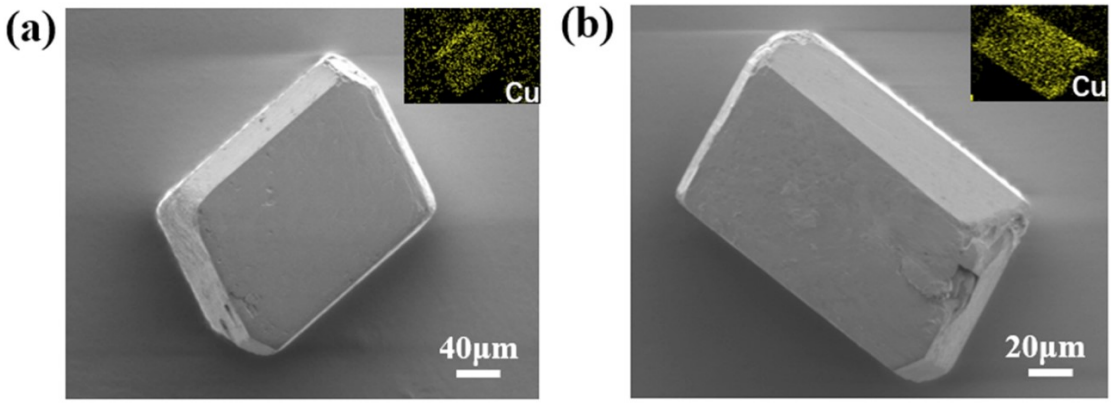

Figure S10. SEM and EDS element mapping images of **(a)** $[Cu_2(OH)_2(Bipy)_2](Hba)_2$ **(b)** $[Cu_2(OH)_2(Phen)_2](pta)$.

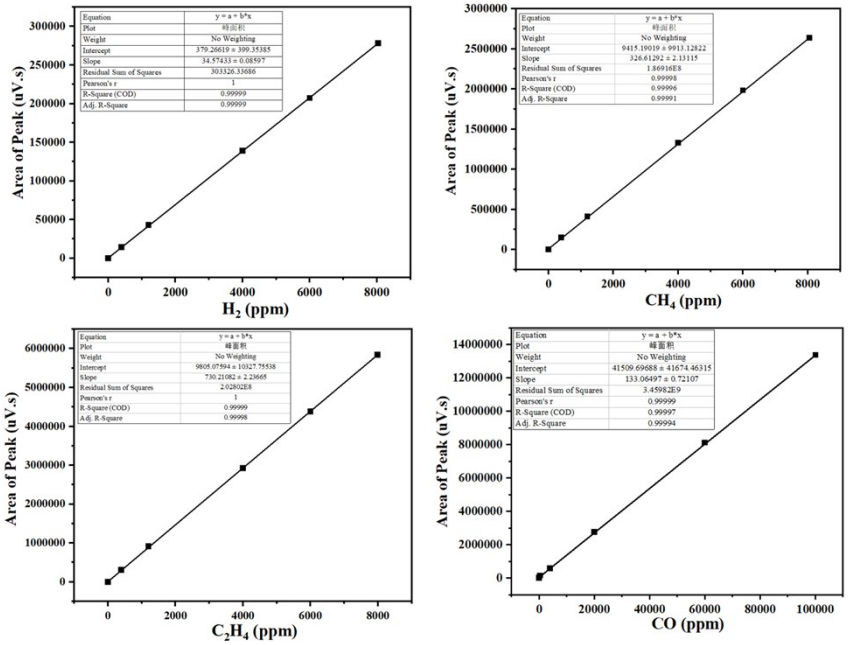

Figure S11. Standard curves of gas products.

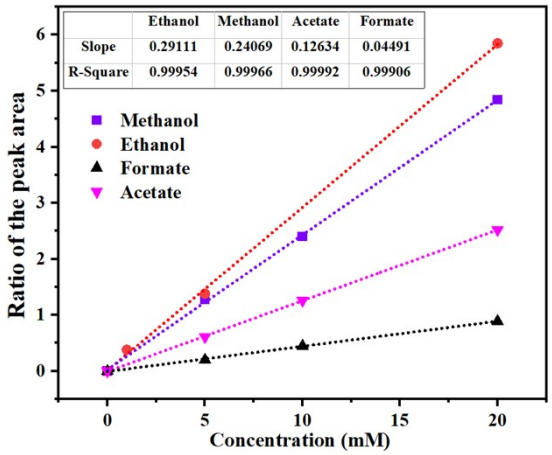

Figure S12. Standard curves of liquid products.

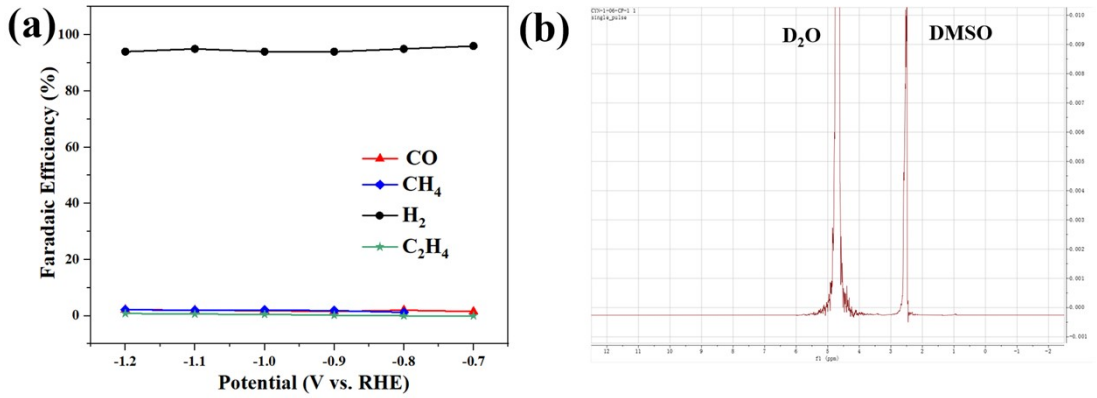

Figure S13. The product distribution of the electrocatalytic CO_2 reduction reaction catalyzed by carbon paper. (a) Faradaic efficiency (FE) of carbon paper at different potentials (−0.7 V to −1.2 V (vs. RHE)). (b) The ^{1}H NMR test results of liquid products of carbon paper.

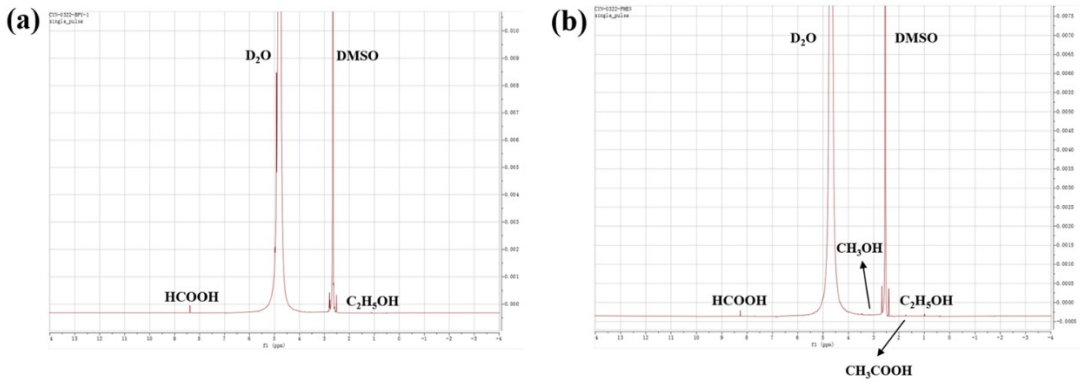

^{1}H NMR: CH_3COOH: 1.76 ppm

CH_3CH_2OH: 1.0 ppm; 3.5ppm

HCOOH: 8.26 ppm

CH_3OH: 3.25 ppm

Figure S14. The ^{1}H NMR test results of liquid products of $[Cu_2(OH)_2L_2]$-X. **(a)** $[Cu_2(OH)_2(Bipy)_2](Hba)_2$ **(b)** $[Cu_2(OH)_2(Phen)_2](pta)$.

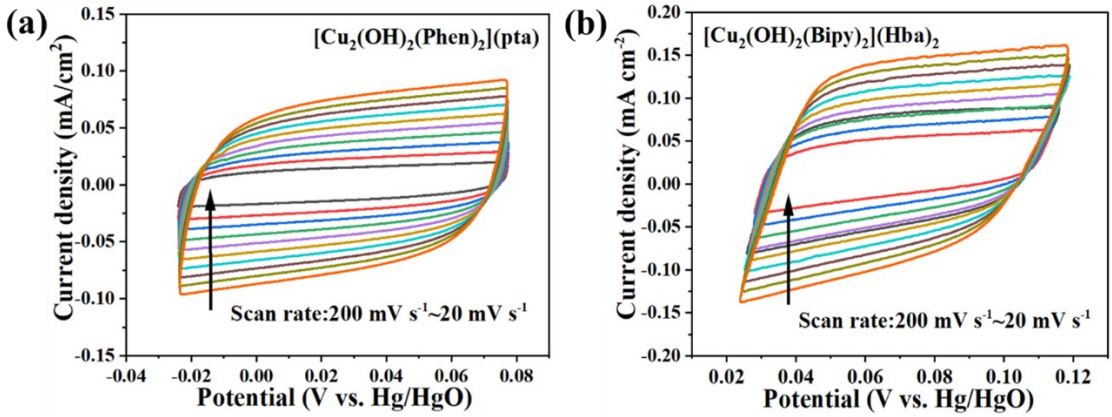

Figure S15. Cyclic voltammetry (CV) curves at various scan rate (20 ~ 200 mV s^{-1}) and corresponding capacitive current of $[Cu_2(OH)_2L_2]$-X. **(a)** $[Cu_2(OH)_2(Phen)_2](pta)$ **(b)** $[Cu_2(OH)_2(Bipy)_2](Hba)_2$.

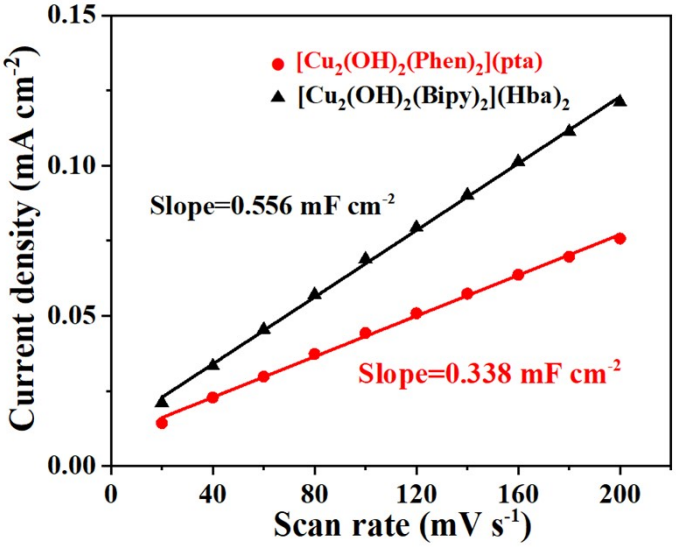

Figure S16. The C_{dl} value of $[Cu_2(OH)_2L_2]$-X.

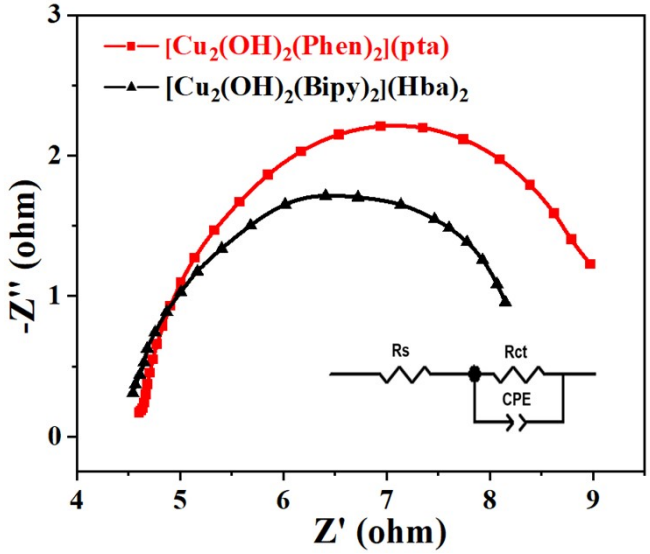

Figure S17. Nyquist plot of $[Cu_2(OH)_2L_2]$-X over the frequency from 0.1 MHz to 0.1 Hz.

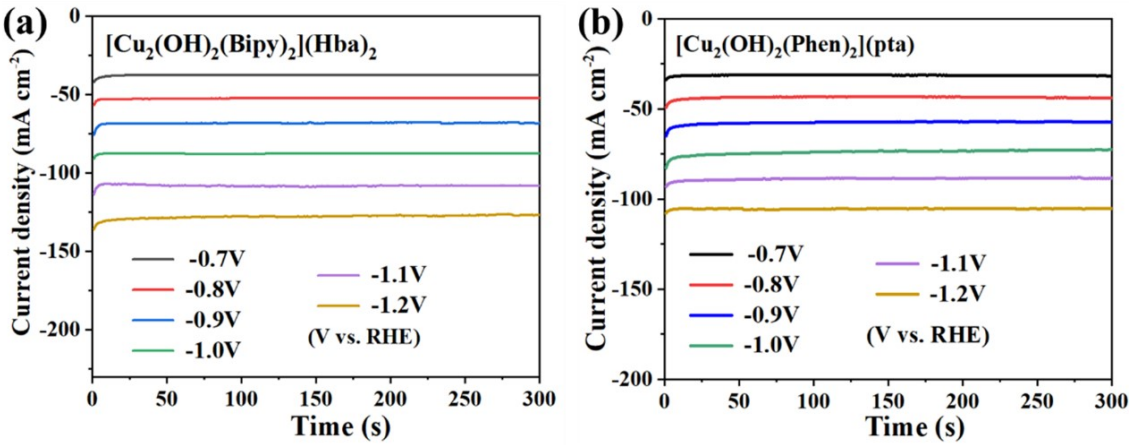

Figure S18. Amperage curves of CO_2 reduction catalyzed by $[Cu_2(OH)_2L_2]$-X in 0.1 M KOH electrolyte at different potentials. **(a)** $[Cu_2(OH)_2(Bipy)_2](Hba)_2$ **(b)** $[Cu_2(OH)_2(Phen)_2](pta)$.

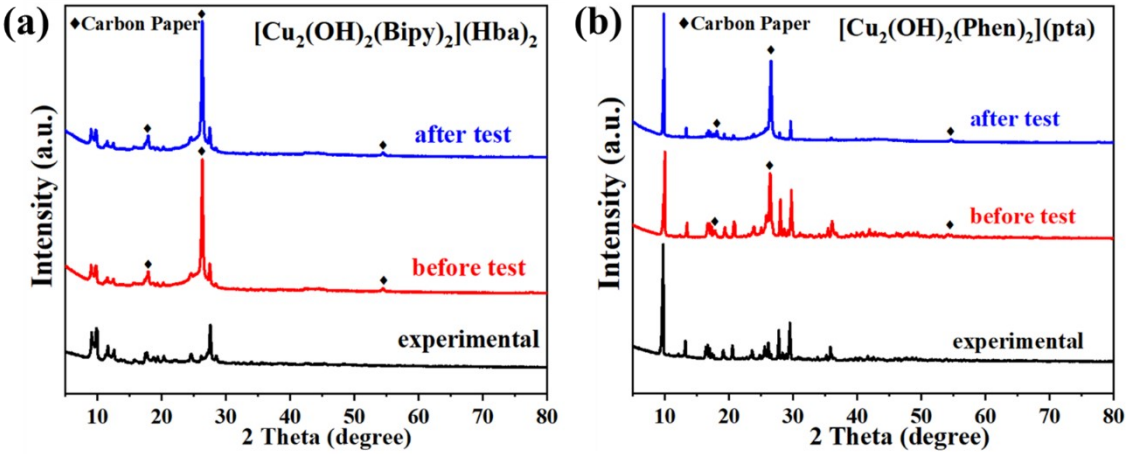

Figure S19. XRD patterns of $[Cu_2(OH)_2L_2]$-X catalysts before and after electrolysis. **(a)** $[Cu_2(OH)_2(Bipy)_2](Hba)_2$ **(b)** $[Cu_2(OH)_2(Phen)_2](pta)$.

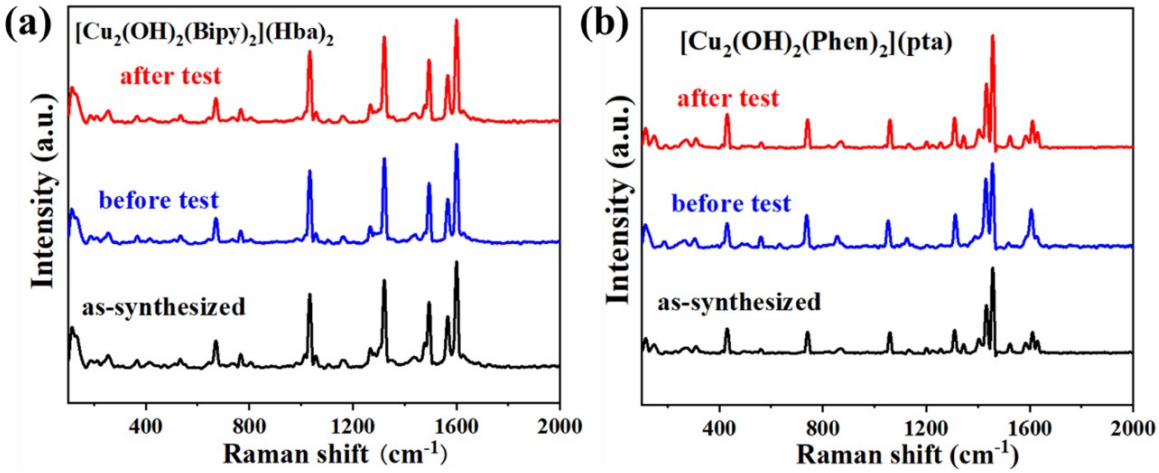

Figure S20. Raman spectra of $[Cu_2(OH)_2L_2]$-X catalysts before and after electrolysis. **(a)** $[Cu_2(OH)_2(Bipy)_2](Hba)_2$ **(b)** $[Cu_2(OH)_2(Phen)_2](pta)$.

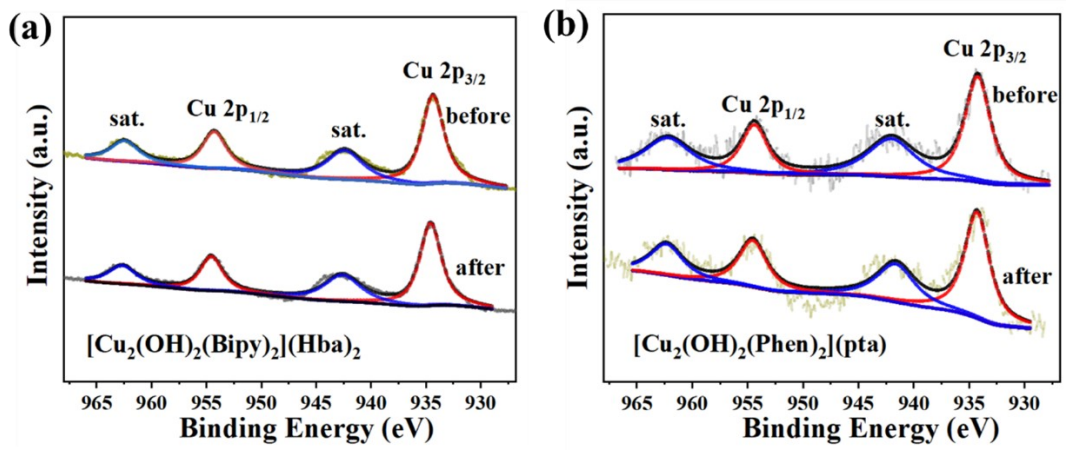

Figure S21. XPS spectra of Cu 2p before and after electrolysis. **(a)** $[Cu_2(OH)_2(Bipy)_2](Hba)_2$ **(b)** $[Cu_2(OH)_2(Phen)_2](pta)$.

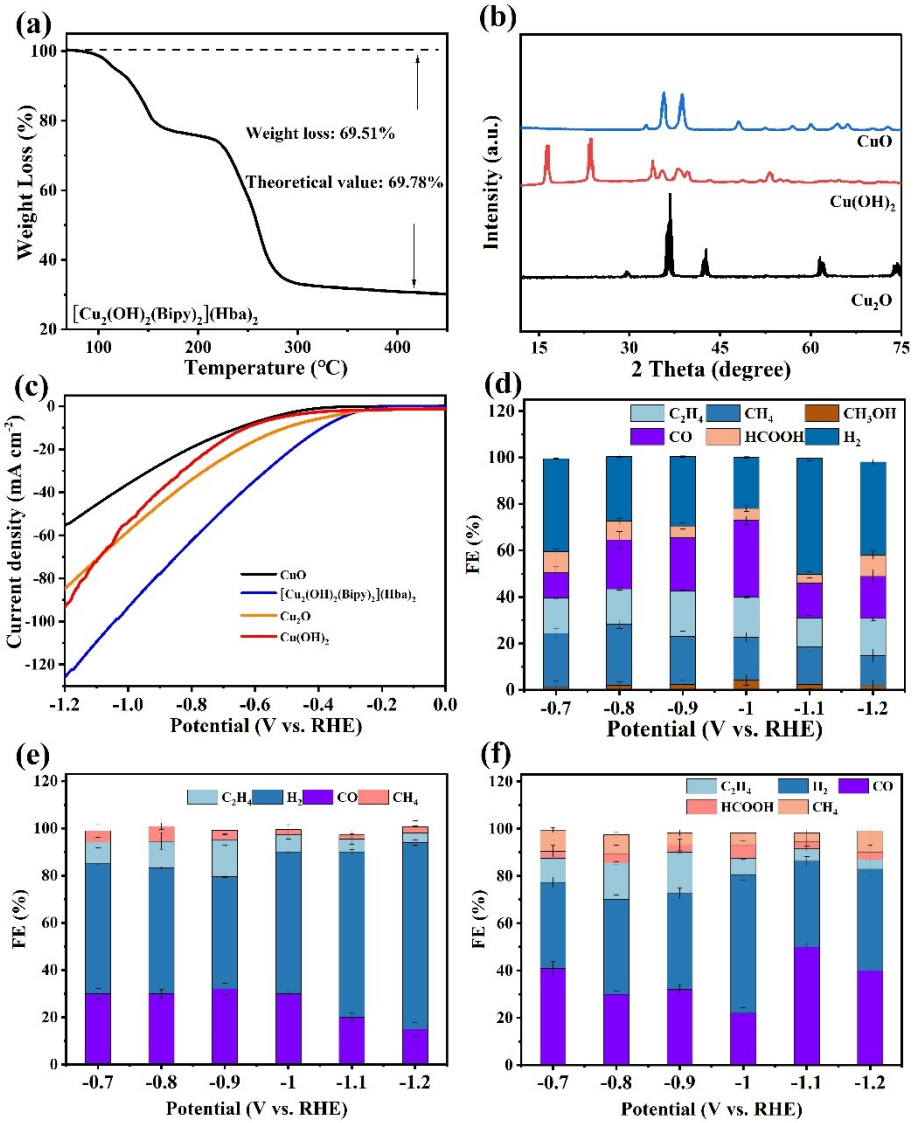

Figure S22 TGA analysis of $[Cu_2(OH)_2(Bipy)_2](Hba)_2$ and the structural characterization of the derived Cu_2O material along with its CO_2RR catalytic performance. (a) TGA curve of $[Cu_2(OH)_2(Bipy)_2](Hba)_2$. (b) X-ray diffraction (XRD) pattern of the material obtained after TGA treatment

of $[Cu_2(OH)_2(Bipy)_2](Hba)_2$; the product was identified as Cu_2O. (c) Linear sweep voltammetry (LSV) test for Cu_2O. (d) Faradaic efficiency of CO_2RR products for Cu_2O. (e) Faradaic efficiency of CO_2RR products for $Cu(OH)_2$. (f) Faradaic efficiency of CO_2RR products for CuO.

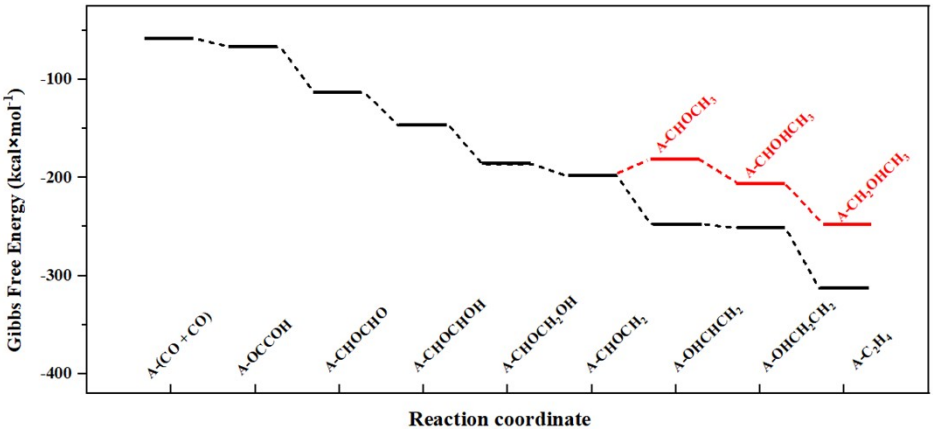

Figure S23 The calculated free energy diagram of CO coupling to form C_2H_4 and C_2H_5OH over the $[Cu_2(OH)_2(Bipy)_2]^{2+}$ model.

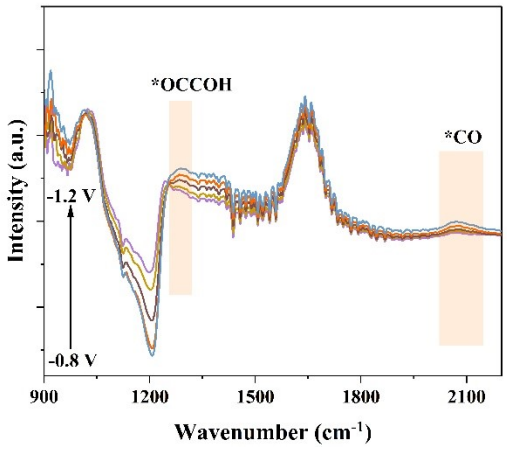

Figure S24. In situ FTIR spectroscopy during CO_2RR on $Cu_2(OH)_2(Bipy)_2$.

Table S1. The predicted distance (H···O) between the hydrogen atom of the intermediates (COOH/CHOCHOH/$CHOCH_2OH$) and the oxygen atom of the bridging ligand (OH^-) and angle (O-H···O) between the OH of the intermediates and the oxygen atom of OH^- in $[Cu_2(OH)_2(Bipy)_2](Hba)_2$ mode structure.

types of intermediates	Distance (Å)	Angle (°)
COOH	1.684	153.45
CO + COOH	1.651	154.15
CHOCHOH	1.585	168.42
$CHOCH_2OH$	1.707	162.52

Table S2. The predicted distance (H···O) between the hydrogen atom of the intermediates (COOH/CHOCHOH/$CHOCH_2OH$) and the oxygen atom of the bridging ligand (OH^-) and angle (O-H···O) between the OH of the intermediates and the oxygen atom of OH^- in $[Cu_2(OH)_2(Phen)_2](pta)$

mode structure.

types of intermediates	Distance (Å)	Angle (°)
COOH	1.679	153.59
CO + COOH	1.648	154.15
CHOCHOH	1.574	169.33
$CHOCH_2OH$	1.694	164.30

Table S3. Crystal data and structure refinement parameters for the $[Cu_2(OH)_2L_2]$-X complexes.

Crystal	$[Cu_2(OH)_2(Bipy)_2](Hba)_2$	$[Cu_2(OH)_2(Phen)_2](pta)$
Chemical formula	$[Cu_2(OH)_2(C_{10}H_8N_2)_2(H_2O)_2](C_4H_3N_2O_3)_2 \cdot 2H_2O$	$[Cu_2(OH)_2(C_{12}H_8N_2)_2(H_2O)_2](C_8H_4O_4) \cdot 8H_2O$
Empirical formula	$C_{28}H_{32}Cu_2N_8O_{12}$	$C_{32}H_{42}Cu_2N_4O_{16}$
CCDC number	2338371	2338368
Formula weight	799.69	865.77
Crystal system	triclinic	triclinic
Space group	$P\bar{1}$	$P\bar{1}$
a (Å)	9.4205(10)	9.2502(15)
b (Å)	10.4548(10)	10.5346(18)
c (Å)	10.7477(11)	11.2002(16)
α (°)	91.627(4)	114.542(5)
β (°)	104.973(4)	112.289(5)
γ (°)	116.069(3)	95.434(6)
V ($Å^3$)	906.19(16)	876.4(2)
Z	2	1
ρ_{calc} (g/cm^3)	1.663	1.640
μ (mm^{-1})	1.264	1.295
F (000)	470.0	448.0
Reflections collected	53471	3061
GOF on F^2	1.099	1.105
$R_1{}^a$ [I＞=2σ(I)]	0.0386	0.0695
$wR_2{}^b$ [I＞=2σ(I)]	0.1041	0.1761
$R_1{}^a$ [all data]	0.0425	0.0718
$wR_2{}^b$ [all data]	0.1068	0.1778
$\Delta\rho_{max}/\Delta\rho_{min}$/e $Å^{-3}$	0.91/0.63	2.26/-0.84

${}^aR_1=\Sigma||F_o|-|F_c||/\Sigma|F_o|$, ${}^bwR_2=|\Sigma w(|F_o|^2-|F_c|^2)|/\Sigma|w(F_o^2)^2|^{1/2}$

Table S4. Selected bond angle (°) and the distance (Å) between Cu1 and $Cu1^2$ atom in $[Cu_2(OH)_2L_2]$-X.

Crystal	Atom1	Atom2	Atom3	Angle (°)	Distance (Å)
$[Cu_2(OH)_2(Bipy)_2](Hba)_2$	Cu1	O1	$Cu1^2$	96.68(5)	2.9097(6)
$[Cu_2(OH)_2(Phen)_2](pta)$	Cu1	O1	$Cu1^2$	96.87(1)	2.8936(1)

Table S5. Faradaic efficiency distributions in liquid products of the $[Cu_2(OH)_2L_2]$-X catalysts.

catalyst	**$[Cu_2(OH)_2(Bipy)_2](Hba)_2$**					
Potential (vs RHE)	**−0.70**	**−0.80**	**−0.90**	**−1.00**	**−1.10**	**−1.20**
FE(CH_3OH)	0.04	0.05	0.01	0.05	0.02	0.03

FE(C_2H_5OH)	0.05	0.12	0.20	0.23	0.20	0.20
FE(HCOOH)	0.25	0.21	0.12	0.12	0.20	0.18
FE(CH_3COOH)	0.06	0.08	0.05	0.07	0.05	0.08
FE (total)	0.40	0.46	0.38	0.47	0.47	0.49

catalyst	**$[Cu_2(OH)_2(Phen)_2](pta)$**					
Potential (vs RHE)	**-0.70**	**-0.80**	**-0.90**	**-1.00**	**-1.10**	**-1.20**
FE(CH_3OH)	0.03	0.04	0.02	0.05	0.02	0.06
FE(C_2H_5OH)	0.04	0.02	0.03	0.06	0.07	0.03
FE(HCOOH)	0.22	0.24	0.20	0.20	0.18	0.23
FE(CH_3COOH)	0.04	0.06	0.05	0.08	0.07	0.09
FE (total)	0.33	0.36	0.30	0.39	0.34	0.41

Table S6. The charge transfer resistance of $[Cu_2(OH)_2L_2]$-X catalysts.

Catalyst	**$[Cu_2(OH)_2(Bipy)_2](Hba)_2$**	**$[Cu_2(OH)_2(Phen)_2](pta)$**
Resistance (Ω)	4.805	5.361

Table S7 Comparison of catalytic performance of some dual-core Cu catalysts

Organic ligand	Catalyst name	Potential (vs RHE)	Current density (mA cm^{-2})	FE(C_2H_4)	Cell type	electrolyte	Ref.
azole	Cutrz	-0.8	280	50	flow	0.1M $KHCO_3$	1
	MAF-2E	-1.3	10.9	51.2	H	0.1M $KHCO_3$	2
	CuBtz	-1.3	7.9	44	H	0.1M $KHCO_3$	3
	NNU-33(H)	-0.7	176.08	27.71	flow	1.0M KOH	4
	Cu-PzH	-1.0	346.46	60	flow	1.0M KOH	5
	Cu3-Br	-0.7	129.58	55.01	flow	0.5M KOH	6
Aromatic acid	S-HKUST-1	-1.32	19.1	60.0	H	0.1M $KHCO_3$	7
Porphyrin	PorCu	-0.976	48	17	H	0.5M $KHCO_3$	8
	CPFs	-1.1	10.2	18	H	0.1M $KHCO_3$	9
	AuNN@PCN-222(Cu)	-1.2	/	52.5	H	0.1M $KHCO_3$	10
Phthalocyanine	PcCu-Cu-O	-1.2	7.3	50	H	0.1M $KHCO_3$	11
	CuPc	-0.95	/	~15	H	0.5M $KHCO_3$	12

Table S8. Calculated Electronic Energies and Gibbs Free Energies in Hartree.

Molecular	Spin state	Electronic energy TPSSh/def-TZVP/SDD (Hartree)	Corrected Gibbs free energy (Hartree)
$[Cu_2(OH)_2(Bipy)_2]^{2+}$	Singlet	-1537.34240342	-1537.0391696
	Triplet	-1537.34692155	-1537.0434741
A-CO_2	Triplet	-1726.00914864	-1725.6985378
A-COOH (with hydrogen bond)	Doublet	-1726.51811901	-1726.195422
	Quartet	-1726.54844244	-1726.2263306
A-COOH (without hydrogen bond)	Quartet	-1726.53306381	-1726.2124411
A-CO	Triplet	-1650.69666039	-1650.3939227
A-(CO + CO_2)	Triplet	-1839.35978945	-1839.0474141
A-(CO + COOH) (with hydrogen bond)	Quartet	-1839.90111902	-1839.5767725
A-(CO + COOH) (without hydrogen bond)	Quartet	-1839.88306221	-1839.5614233
A-(CO + CO)	Triplet	-1764.05140654	-1763.7472391
A-CHOCO	Quartet	-1764.63159563	-1764.3086047
A-CHOCHO	Triplet	-1765.26653698	-1764.9310176
A-CHOCHOH (with hydrogen bond)	Quartet	-1765.88244553	-1765.532764
A-CHOCHOH (without hydrogen bond)	Quartet	-1765.86680102	-1765.5191558
A-$CHOCH_2OH$ (with hydrogen bond)	Triplet	-1766.50515509	-1766.1442687
A-$CHOCH_2OH$ (without hydrogen bond)	Triplet	-1766.49778805	-1766.1391056
A-$CHOCH_2$	Quartet	-1690.59732087	-1690.2553025
A-$CHOHCH_2$	Triplet	-1691.23782076	-1690.881838
A-CH_2OHCH_2	Quartet	-1691.80145613	-1691.4359813
A-C_2H_4	Triplet	-1615.97741402	-1615.6265885
A-(CO_2 + $2H_2O$)	Triplet	-1878.95951903	-1878.6028049
A-(COOH + $2H_2O$)	Quartet	-1879.49868634	-1879.1300474
$[Cu_2(OH)_2(Phen)_2]^{2+}$	Triplet	-1689.8773946	-1689.5484212
B-CO_2	Triplet	-1878.53905442	-1878.2030085
B-COOH	Quartet	-1879.07877776	-1878.7310326
B-CO	Triplet	-1803.22774287	-1802.899284
B-(CO + CO_2)	Triplet	-1991.89046131	-1991.5538061

B-(CO + COOH)	Quartet	-1992.43140344	-1992.0814156
B-(CO + CO)	Triplet	-1916.58109371	-1916.2518553
B-CHOCO	Quartet	-1917.16222751	-1916.8136105
B-CHOCHO	Triplet	-1917.79689602	-1917.4357683
B-CHOCHOH	Quartet	-1918.41318958	-1918.0379126
B-$CHOCH_2OH$	Triplet	-1919.03561014	-1918.6490772
B-$CHOCH_2$	Quartet	-1843.12787374	-1842.7601676
B-$CHOHCH_2$	Triplet	-1843.76827673	-1843.3866311
B-CH_2OHCH_2	Quartet	-1844.33195974	-1843.9409031
B-C_2H_4	Triplet	-1768.5076417	-1768.1313001
CO_2(g)	Singlet	-188.657974555	-188.6681332
C_2H_4(g)	Singlet	-78.6245968548	-78.5944516
H_2O(g)	Singlet	-76.4671537817	-76.4632079
H_2(g)	Singlet	-1.17890651595	-1.1804514

References

[1] Golovnev, N. N., Molokeev, M. S., Sterkhova, I. V., & Lesnikov, M. K, Crystal structures of $[Cu_2(2,2'\text{-bipyridine-}N,N')_2(H_2O)_2(\mu_2\text{-}OH)_2](\text{barbiturate})_2\cdot 2H_2O$ and $[Cu(2,2'\text{-bipyridine-}N,N')(H_2O)(\text{barbiturate-}O)Cl]\cdot 2H_2O$, Inorg. Chem. Commun. 97 (2018) 88-92.

[2] X. Li, D.-Y. Cheng, J.-L. Lin, Z.-F. Li, Y.-Q. Zheng, Di-, Tetra-, and Hexanuclear Hydroxy-Bridged Copper (II) Cluster Compounds: Syntheses, Structures, and Properties, Cryst. Growth Des. 8 (2008) 2853-2861.

[3] Dolomanov, O. V., Bourhis, L. J., Gildea, R. J., Howard, J. A., Puschmann, H, OLEX2: a complete structure solution, refinement and analysis program. J. Appl. Cryst. 42 (2009) 339-341.

[4] Sheldrick G. M, Acta Cryst. 2015, A71, 3-8.

[5] Frisch, M. J.; Trucks, G. W.; Schlegel, H. B.; Scuseria, G. E.; Robb, M. A.; Cheeseman, J. R.; Scalmani, G.; Barone, V.; Mennucci, B.; Petersson, G. A.; Nakatsuji, H.; Caricato, M.; Li, X.; Hratchian, H. P.; Izmaylov, A. F.; Bloino, J.; Zheng, G.; Sonnenberg, J. L.; Hada,

M.; Ehara, M.; Toyota, K.; Fukuda, R.; Hasegawa, J.; Ishida, M.; Nakajima, T.; Honda, Y.; Kitao, O.; Nakai, H.; Vreven, T.; Montgomery, J. A., Jr.; Peralta, J. E.; Ogliaro, F.; Bearpark, M.; Heyd, J. J.; Brothers, E.; Kudin, K. N.; Staroverov, V. N.; Kobayashi, R.; Normand, J.; Raghavachari, K.; Rendell, A.; Burant, J. C.; Iyengar, S. S.; Tomasi, J.; Cossi, M.; Rega, N.; Millam, J. M.; Klene, M.; Knox, J. E.; Cross, J. B.; Bakken, V.; Adamo, C.; Jaramillo, J.; Gomperts, R.; Stratmann, R. E.; Yazyev, O.; Austin, A. J.; Cammi, R.; Pomelli, C.; Ochterski, J. W.; Martin, R. L.; Morokuma, K.; Zakrzewski, V. G.; Voth, G. A.; Salvador, P.; Dannenberg, J. J.; Dapprich, S.; Daniels, A. D.; Farkas, O.; Foresman, J. B.; Ortiz, J. V.; Cioslowski, J.; Fox, D. J. Gaussian 09, Revision A.01; Gaussian, Inc.: Wallingford CT, 2009.

[6] Li, X.; Panetier, J. A, Computational Study for CO_2-to-CO Conversion over Proton Reduction Using $[Re[BpyMe(Im\text{-}R)](CO)_3Cl]^+$ (R = Me, Me_2, and Me_4) Electrocatalysts and Comparison with Manganese Analogues. ACS Catal. 11 (2021) 12989–13000.

[7] Shi, L.-L.; Li, M.; You, B.; Liao, R.-Z, Theoretical Study on the Electro-Reduction of Carbon Dioxide to Methanol Catalyzed by Cobalt Phthalocyanine, Inorg. Chem. 61 (2022) 16549–16564.

[8] Deng, Y.; Zhao, J.; Wang, S.; Chen, R.; Ding, J.; Tsai, H.-J.; Zeng, W.-J.; Hung, S.-F.; Xu, W.; Wang, J.; Jaouen, F.; Li, X.; Huang, Y.; Liu, B, Operando Spectroscopic Analysis of Axial Oxygen-Coordinated Single-Sn-Atom Sites for Electrochemical CO_2 Reduction, J. Am. Chem. Soc. 145 (2023) 7242–7251.

[9] Zhang, H.; Xu, C.; Zhan, X.; Yu, Y.; Zhang, K.; Luo, Q.; Gao, S.; Yang, J.; Xie, Y, Mechanistic Insights into CO_2 Conversion Chemistry of Copper Bis-(Terpyridine)

Molecular Electrocatalyst Using Accessible Operando Spectrochemistry, Nat. Commun. 13 (2022) 6029.

[10] Adamo, C.; Barone, V, Toward Reliable Density Functional Methods Without Adjustable Parameters: The PBE0 Model. J. Chem. Phys. 110 (1999) 6158−6170.

[11] Weigend, F.; Ahlrichs, R, Balanced Basis Sets of Split Valence, Triple Zeta Valence and Quadruple Zeta Valence Quality for H to Rn: Design and Assessment of Accuracy, Phys. Chem. Chem. Phys. 7 (2005) 3297−3305.

[12] Weigend, F, Accurate Coulomb-Fitting Basis Sets for H to Rn, Phys. Chem. Chem. Phys. 8 (2006) 1057.

[13] Dolg, M.; Wedig, U.; Stoll, H.; Preuss, H, Energy-adjusted ab initio pseudopotentials for the first row transition elements, J. Chem. Phys. 86 (1987) 866−872.

[14] Grimme, S.; Ehrlich, S.; Goerigk, L, Effect of the Damping Function in Dispersion Corrected Density Functional Theory. J. Comput. Chem. 32 (2011) 1456−1465.

[15] Staroverov, V. N.; Scuseria, G. E.; Tao, J.; Perdew, J. P, Comparative Assessment of a New Nonempirical Density Functional: Molecules and Hydrogen-Bonded Complexes, J. Chem. Phys. 119 (2003) 12129−12137.

[16] Schäfer, A.; Huber, C.; Ahlrichs, R. Fully Optimized Contracted Gaussian Basis Sets of Triple Zeta Valence Quality for Atoms Li to Kr, J. Chem. Phys. 100 (1994) 5829−5835.

[17] Marenich, A. V.; Cramer, C. J.; Truhlar, D. G, Performance of SM6, SM8, and SMD on the SAMPL1 test set for the prediction of small-molecule solvation free energies, J. Phys. Chem. B 113 (2009) 4538−4543.

[18] Marenich, A. V.; Cramer, C. J.; Truhlar, D. G, Universal solvation model based on solute electron density and on a continuum model of the solvent defined by the bulk dielectric constant and atomic surface tensions, J. Phys. Chem. B 113 (2009) 6378−6396.

[19] Maurer, L. R.; Bursch, M.; Grimme, S.; Hansen, A, Assessing Density Functional Theory for Chemically Relevant Open-Shell Transition Metal Reactions, J. Chem. Theory Comput. 17 (2021) 6134–6151.

[20] Borrego, E.; Tiessler-Sala, L.; Lázaro, J. J.; Caballero, A.; Pérez, P. J.; Lledós, A, Direct Benzene Hydroxylation with Dioxygen Induced by Copper Complexes: Uncovering the Active Species by DFT Calculations. Organometallics 41 (2022) 1892–1904.

[21] V.A. Larionov, L. V. Yashkina, M.G. Medvedev, A.F. Smol'yakov, A.S. Peregudov, A.A. Pavlov, D.B. Eremin, T.F. Savel'yeva, V.I. Maleev, Y.N. Belokon, Henry Reaction Revisited. Crucial Role of Water in an Asymmetric Henry Reaction Catalyzed by Chiral NNO-Type Copper(II) Complexes, Inorganic Chemistry. 58 (2019) 11051–11065.

[22] S. Khan, S. Herrero, R. Gonzalez-Prieto, M.G.B. Drew, S. Banerjee, S. Chattopadhyay, New J. Chem. 42 (2018) 13512–13519

[23] T. Lu, Q. Chen, Shermo: A general code for calculating molecular thermochemistry properties, Comput. Theor. Chem. 1200 (2021) 113249.

[24] S. Grimme, Supramolecular Binding Thermodynamics by Dispersion-Corrected Density Functional Theory, Chem.-Eur. J. 18 (2012) 9955.